# Exploring the thumbprints of Ag-hydroxyapatite composite as a surface coating bone material for the implants

J. Anita Lett, Suresh Sagadevan, Suriati Paiman, Faruq Mohammad, Romana Schirhagl, Estelle Léonard, Solhe Alshahateet, Won-Chun Oh

# Exploring the thumbprints of Ag-hydroxyapatite composite as a surface coating bone material for the implants

Lett, J. Anita; Sagadevan, Suresh; Paiman, Suriati; Mohammad, Faruq; Schirhagl, Romana; Leonard, Estelle; Alshahateet, Solhe F.; Oh, Won-Chun

*Published in:*
Journal of Materials Research and Technology

*DOI:*
10.1016/j.jmrt.2020.09.037



*Publication date:*
2020

Available online at www.sciencedirect.com

jmr&t Journal of Materials Research and Technology

https://www.journals.elsevier.com/journal-of-materials-research-and-technology

Original Article

# Exploring the thumbprints of Ag-hydroxyapatite composite as a surface coating bone material for the implants

*J. Anita Lett*[a,*], *Suresh Sagadevan*[b,*], *Suriati Paiman*[c], *Faruq Mohammad*[d], *Romana Schirhagl*[e], *Estelle Léonard*[f], *Solhe F. Alshahateet*[g], *Won-Chun Oh*[h,*]

[a] *Department of Physics, Sathyabama Institute of Science and Technology, Chennai, Tamil Nadu, India*
[b] *Nanotechnology & Catalysis Research Centre, University of Malaya, Kuala Lumpur 50603, Malaysia*
[c] *Department of Physics, Faculty of Science, Universiti Putra Malaysia, 43400 Serdang, Selangor, Malaysia*
[d] *Surfactant Research Chair, Department of Chemistry, College of Science, King Saud University, P.O. Box 2455, Riyadh, Kingdom of Saudi Arabia 11451*
[e] *Groningen University, University Medical Center Groningen, Antonius Deusinglaan 1, 9713 AW Groningen, Netherlands*
[f] *ESCOM, UTC, EA TIMR 4297, 1 allée du Réseau Jean-Marie Buckmaster, 60200 Compiègne, France*
[g] *Department of Chemistry, Mutah University, P.O.BOX 7, Mutah, 61710 Karak, Jordan*
[h] *Department of Advanced Materials Science and Engineering, Hanseo University, Seosan-si, Chungnam 356-706, Republic of Korea*

ARTICLE INFO

*Article history:*
Received 30 June 2020
Accepted 7 September 2020
Available online 21 September 2020

*Keywords:*
Polylactic acid scaffolds
Silver doped hydroxyapatite
Fused deposition method
Antibacterial studies
Hemocompatibility
Hardness study

ABSTRACT

Polylactic acid (PLA), although has many interesting physicochemical characteristics, the strong hydrophobicity and a lack of antibacterial activity restricting its widespread application in the medical sector. In a view of addressing some of the limitations of PLA, the current study aimed to test the antibacterial efficacy of active metal-doped bioceramic/PLA composite formed by the fused deposition manufacturing (FDM) technique. For the testing, we prepared polyvinyl alcohol (PVA) bound silver-hydroxyapatite (Ag-HAp) composite and further applied as a low-temperature coating onto the PLA scaffold designed for the appropriate cell development, differentiation, and bio-mineral establishment. From the analysis, we revealed that the larger surface area of three-dimensional (3D) printed composite material having the matrix porosity makes it a perfect biocompatible material with no loss to its mechanical potency. The HAp/PLA and Ag-HAp/PLA composites were tested for the hemocompatibility, and antibacterial activity (gram-positive and gram-negative bacteria). Further, the mechanical property of the Ag-HAp/PLA scaffold was tested. The results demonstrated that the Ag-HAp/PLA composite offers the biocompatibility and antibacterial ability and therefore can serve as the potential bone implant material.



* *Corresponding authors.*
E-mails: anitalett2014@gmail.com (J.A. Lett), drsureshnano@gmail.com (S. Sagadevan), wc_oh@hanseo.ac.kr (W. Oh).
https://doi.org/10.1016/j.jmrt.2020.09.037

## 1. Introduction

Additive manufacturing (AM), commonly known as three-dimensional (3D) printing offers a range of fascinating pathways for the fabrication of composite materials over other monolithic prototyping. Thus, by making use of this AM technique, several biomaterials are being fabricated like tissue engineering [1,2], soft composites [3], ceramics [4], magnetic materials [5], and direct biological material printings [6]. Based on the application, this technique can particularly be helpful in the biomedical sector for the regeneration of defective bone tissues caused because of accidents or surgical amputation of tumors [7]. Since the usage of synthetic materials for the development of bone implants helps to reconstruct the bone tissues with strong structural support and no loss to the interferences of biological tissue [8,9]. To serve for such behavior, the biodegradable matrices are indicated to provide momentary scaffolds within which the bone tissues can regenerate. Among many different polymers, polylactic acid (PLA) offers excellent biocompatibility, biodegradability, non-toxicity, and mechanical strength and hence finds its usage in many different clinical applications like drug delivery systems, surgical stitches, medical implantable devices etc. [10].

Fused deposition manufacturing (FDM) is the most frequently used practice for the construction of pure plastic parts with low costs, negligible wastes, and simplicity with material switching [11,12]. PLA is one of the most encouraging synthetic polymers that can be used as a source biomaterial in the FDM technique and is due to the fact that it can undergo degradation in the aqueous medium and is biocompatible in the biological surrounding [12]. In general, the mechanical properties of pure PLA scaffolds are comparable with the natural bone and so, it can be used for craniofacial bone restoration and cranial defects [10]. Conversely, the PLA has strong hydrophobicity that limits its extensive application in medicine and so there is a strong need for the ideal bio implantable scaffold material that can facilitate the growth and activity of cells like cell adhesion, proliferation, and functional differentiation [13]. Besides that, it must be bioactive or bioresorbable with adequate mechanical property to endure stress states that might appear at the implanted site. In that way, the implantable scaffold can act as extracellular matrix (ECM) for tissue rejuvenation. In recent works by Alvarez-Barreto et al. [14] fabricated Arg—Gly–Asp-modified PLA scaffolds to regulate the cell characteristics and progress tissue functioning for a better and well-organized tissue engineering approaches. The deposited CaP ceramic over PLA nanofibrous scaffolds was comparable to the constituents of natural bone, but not able to achieve the desired osteoinduction [15]. Bearing in mind that the main constituents of natural bone are collagen fibers and hydroxyapatite (HAp) crystals, and in that way, the nano-HAp has excellent properties such as biocompatibility and bioactivity that are crucial for cell development [9]. Consequently, the inorganic/organic composite materials enclose a greater potential for bone tissue engineering applications. Numerous scaffolds have been fabricated by directly mixing the composite active additives but leads to uncontrolled homogeneity in the polymer matrix [12].

In our day today life deals with various viruses, fungi, and bacteria and thus, the manufactured HAp implantable material should not allow any of these microorganisms to grow on its surface. The synthetic HAp does not exhibit any antibacterial property and thus it becomes important to modify its surface with active bacteriostatic elements like Ag, Sr, Zn, Ce, Ti, etc [16,17]. As an example, the presence of Ag metal with active antibacterial property can easily damage the bacterial cell wall, as well as bind to the DNA and RNA of bacteria and thereby preventing the growth that finally results in bacterial annihilation [18]. Besides, the radius of $Ag^{+}$ atom is 0.126 nm which is almost the same as the radius of $Ca^{2+}$ atom (0.100 nm), therefore under some conditions, the Ag ions can be replaced by the Ca ions in the HAp crystal lattice. Therefore, to advance the biomedical and clinical uses of HAp, it is very essential to incorporate Ag ions into the HAp's crystal lattice and in that view, some of the researchers have focused on developing HAp-based composite coatings [19,20].

By taking advantage of the bioceramic properties of HAp to serve as a natural bone and Ag's antibacterial properties, we have incorporated $Ag^{+}$ ions into the HAp crystals to form Ag-HAp and further surface modified with PLA scaffolds using PVA (polyvinyl alcohol) to finally generate Ag-HAp/PLA scaffold. The highlights of the study reported here include the fabrication of required interconnected porous PLA scaffolds by the FDM technique using appropriate CAD design. Thus, the prepared HAP/PLA,Ag-HAp/PLA composites and scaffold were characterized for the micro-structure, crystallinity, elemental composition, mechanical properties, biocompatibility, and antibacterial efficacy.

## 2. Materials and methods

### 2.1. 3D printing of PLA frameworks

The CAD models for the PLA scaffolds were designed using Catia design software and fabricated by a Creality Ender-3 pro-High Precision 3D printer by Shape tool 3D Technology FSD machine. Before the FDM process, the STL (Standard Tessellation Language) file created by the CAD software is fragmented into thin horizontal slices and the width of each layer can be driven as per the requirement [21]. Fig. 1 shows the FDM printer, printing process, and the formed material.

### 2.2. Synthesis of Ag-doped HAp

For the formation of Ag-Hap particles, the precursors used include the analytical reagent grade calcium nitrate tetrahydrate; $Ca(NO_3)_2{\cdot}4H_2O$, ammonium dihydrogen phosphate; $(NH_4)H_2PO_4$, and silver nitrate; $AgNO_3$ (Merck, Mumbai, Maharashtra, India). During the synthesis, we first formed nano-HAp by simply dissolving the calcium and phosphate solutions above pH 10 to undergo the precipitation process. In this process, the common practice requires the use of a stoichiometric ratio of Ca:P to be 1.67 and involves the dropwise addition of one reagent to the other with continuous stirring under an inert atmosphere. This results in the generation of a suspension under atmospheric temperature, which on washing, drying, and smashing forms the nano-powder of HAp.

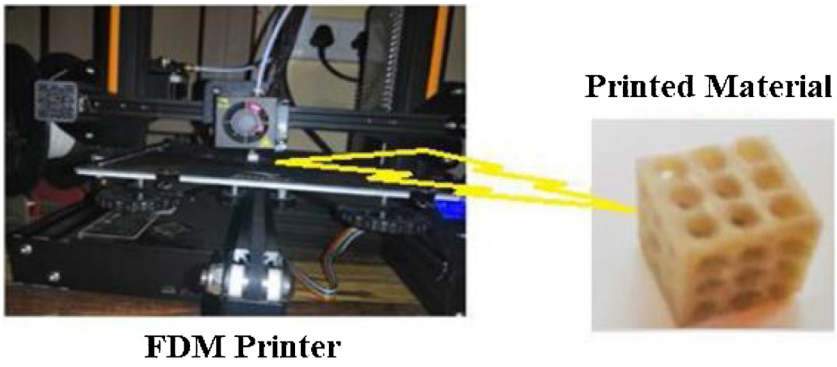


**Fig. 1 – Schematic representation of the FDM printing process for the formation of PLA porous scaffolds.**

For the synthesis of Ag-doped HAp, 0.45 M of $Ca(NO_3)_2{\cdot}4H_2O$ along with 0.05 M of $AgNO_3$ was first dissolved in distilled water and adjusted to a total volume of 250 mL and kept in a conical flask. Similarly, a 250 mL volume of 0.3 M of $(NH_4)H_2PO_4$ was prepared separately using distilled water and transferred to a burette. On mixing of both solutions at a flow rate of 3 mL/min, room temperature, and stirring for 3 h results in the formation of a milky white solution (having the stoichiometric ratio of 1.67). The whole process pH was maintained at 11 (>10) by the dropwise addition of ammonia to $Ca(NO_3)_2{\cdot}4H_2O + AgNO_3$ solution. The white coloured solution was kept at room temperature overnight, followed by washing thrice with distilled water, subjected to calcination at 100°C for 3 h, and finally sintered at 500°C to obtain Ag-HAp composite.

### 2.3. *Incorporation of Ag-HAp composite onto the 3D PLA frameworks*

For the surface modification of Ag-HAp composite at low-temperature conditions, we have used PLA scaffolds and for effective bonding, polyvinyl alcohol (PVA) was employed as the binding agent. For the surface modification reaction, about 1 g of PVA (analytical grade) was mixed to 50 mL of distilled water, stirred using a magnetic stirrer at 50 °C to form a homogenous solution. Now, the Ag-HAp composite dispersed in ethanol was added to the PVA solution, while stirring for another 2 h, and after the period, the FDM printed PLA scaffolds were immersed and kept in the PVA solution for 24 h. At the end of the incubation period, both the parts were removed, allowed to drip-dry, and then placed in an air dryer maintained at 50 °C for one week to obtain the final product of Ag-HAp/PLA scaffold.

## 3. Characteristic techniques

### 3.1. *Morphological and structural characterization*

The morphological organization and surface nature of samples were observed using the field emission scanning electron microscopy (FESEM; JMS7500 F; JEOL, Tokyo, Japan) and high-resolution transmission electron microscopy (HRTEM: FEI-TECNAI G2-200 kV TWIN). The energy-dispersive X-ray (EDX: X-Max, USA) analysis with a regular unit (Oxford Instruments, UK) connected to the FESEM instrument was employed for the elemental mapping and composition of elements in the composite. For the sampling, the testing materials were first dispersed in ethanol, sonicated, and then placed a drop of suspension onto the cleaned aluminum foil, dried at atmospheric air, and was sputter-coated with gold (Edwards Sputter Coater S150B, London, UK). Similarly, the powder X-ray diffraction (XRD) analysis (Bruker-D8 powder diffractometer, Bruker AXS GmbH, Karlsruhe, Germany), Fourier transform infrared (FTIR) spectroscopy (from Agilent Cary 630, Agilent Technologies, Santa Clara, CA, USA), and X-ray photoelectron spectroscopy (XPS; SSX-100 spectrometer) having monochromatized X-ray beam Al Kα radiation (operating at 1486.6 eV) were employed for the other characterizations.

### 3.2. *Biocompatibility studies*

#### 3.2.1. *Measurement of FBS adsorption onto the HAp samples*

The biocompatibility of HAp and Ag-HAp/PLA composite was assessed by the protein adsorption assay and for the analysis, the testing pellets (at a dimension 10 × 1 mm dia) were engrossed in tris buffer at pH 7.4 for a 20 h period. Then, the scaffolds were incubated in Minimum Essential Medium (α-MEM) containing 10% Fetal Bovine Serum (FBS; synthetic cell culture media) for 4 h. At the end of the incubation period, the scaffolds were first rinsed thoroughly with an isotonic tris buffer solution, and then the surface was exposed to a 2% sodium dodecyl sulfate (SDS) solution for 24 h to elude any adsorbed proteins. The total capacity of adsorbed protein was investigated using the BCA protein assay equipment having the microplate reader (Molecular Devices LLC, Sunnyvale, CA, USA).

#### 3.2.2. *Hemolytic studies*

The hemocompatibility of HAp and Ag-HAp/PLA composite was examined as per the earlier procedure described by Lv et al. [22]. Briefly, about 1.25 mL of sterile saline was first combined with 1 mg of testing sample (HAp or Ag-HAp/PLA composite powder) and in a separate tube, 4 mL volume of blood collected from the healthy human was diluted with that of 5 mL sterile saline solution. From this, 20 μL of diluted blood solution was collected and mixed with that of a testing sample containing tube and further incubated at 37 °C for

30 min and then all the tubes were incubated for 60 min at 37°C in a shaking water bath. The release of hemoglobin was determined after centrifugation by photometric analysis of the supernatant at 540 nm using the UV spectrophotometer (Shimadzu UV 2450) and further the hemolytic rate (HR) was calculated from the Eq. (1),

$$HR = [(D_t - D_{nc})/(D_{pc} - D_{nc})] \times 100\% \quad (1)$$

where $D_t$, $D_{nc}$, and $D_{pc}$ corresponds to the absorbances of the testing sample, negative control, and positive control, respectively.

### 3.3. *Antibacterial studies*

For the testing, the samples were made into pellets of 10 mm diameter and 2 mm thickness. To accomplish the study, sterile Petri-dishes (90 mm diameter) comprising sterile nutrient agar medium (15 mL) were taken. After 24 h of bacterial culture, the just prepared bacterial inoculums were spread over the entire surface of agar medium thrice using a sterile cotton swab, to make sure that the bacterial culture is thoroughly and evenly distributed on the surface of plates. The test samples were bored in the medium in each plate and the plates were preserved at normal room temperature for 45 min and further incubated at 37 °C for 24 h. Finally, the diameter of the zone of inhibition (mm) was measured at 3-equidistant places taken from the center of the inhibition zone, and the average of these three values was taken as the final. All procedures were in co-operated in triplicate.

### 3.4. *Hardness study*

For this, the compressive tests were carried out on a 10 × 10 mm dimension of PLA-coated HAp and Ag-HAp/PLA scaffold by making use of the Universal testing machine (INSTRON 5566, Germany) with a maximum compression load cell of 10 kN and a cross-head speed of 1.0 mm/min.

## 4. Results and discussion

The mineralized Ag-HAp/PLA porous scaffolds in this work used a low-temperature process to modify the PLA surface as compared to the plasma-sprayed coating that requires elevated temperatures. The use of mineralized Ag-HAp along with PVA as a biocompatible binder on the surface of PLA porous scaffolds under physiological conditions in a more rapid and simple method to emerge exquisite crystal morphology for cell growth. Fig. 2 shows the comparison of the powder XRD pattern of pure HAp and Ag-HAp composite, and from the figure, the remarkable peaks identified at the 2θ of 31.74, 32.18, and 32.89 can be indexed to the HAp material and also matches well with the JCPDS card # 89-6495. The very feeble peak for silver associated at 2$\theta$ of 38.1 and 44.2 (JCPDS card No. 4–783) are also found. The sharp peaks of the HAp sample indicate its highly crystalline nature (5.16%); whereas, the Ag-doped silver HAp peaks are broad signifying the change (decrease) in crystallite size (34.8 nm) and hence the crystallinity (1.95%) of the doped sample [23]. The addition

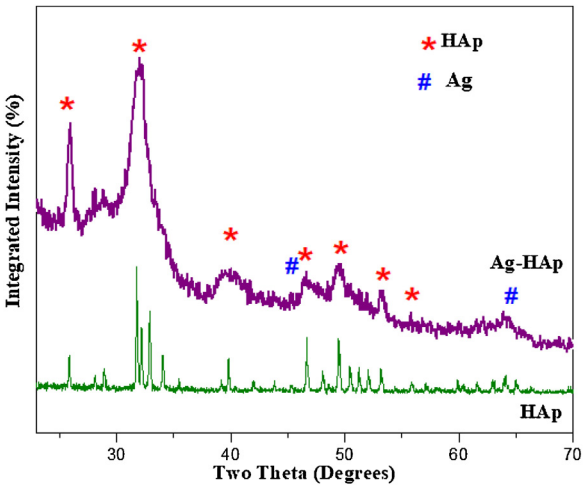


**Fig. 2 – Comparison of the powder XRD pattern of HAp and Ag-HAp nanopowder.**

**Table 1 – Comparison of the crystallinity data for the Hap before and after doping with Ag metal.**

| Sample | The crystallite size (nm) | Crystallinity (%) |
|---|---|---|
| HAp | 71 | 5.16 |
| Ag-HAp | 34.8 | 1.95 |

of silver nitrate (0.05 M of silver nitrate solutions into calcium nitrate solution) results in the replacement of Ca in HAp with Ag ions and thus leads to the distortion of HAp lattice resulting in the formation of amorphous nature. We observed significantly no difference from the XRD pattern, and it could due to the preferred orientation of doped elements (Ag) concentration as low [24]; the trace quantity of metal nitride dopant could not be able to produce a considerable impact in the XRD pattern. Since the dopant concentration is low, the impact of the peaks in the XRD pattern is very feeble and hardly detected due to the lower instrumental detection limit (Table 1).

The analysis of composites by the XPS technique is commonly used for the surface analysis and to detect trace elements (except hydrogen) along with their oxidation states in an unknown material. Fig. 3 represents the XPS survey and the Ag elemental spectrum of the Ag-HAp composite. The survey spectrum predicts the presence of major constituents for the elements of Ca, P, Ag, C, and O of Ag-HAp composite. From the spectra, we observed the peaks at the binding energy positions of 348 eV and 351 eV that can be attributed to the Ca $2p_{3/2}$ and Ca $2p_{1/2}$, respectively [25]. Similarly, the other peaks observed corresponding to the binding energies of 190 eV, 531 eV, and 532.2 eV corresponds to P 2s, O 1s elements of the oxygen atoms associated with the phosphate group and adsorbed water respectively in Ag-HAp [26]. The minuscule peak found obviously at 368.2 and 374.3 eV corresponds to Ag $3d_{3/2}$ and Ag $3d_{5/2}$ agrees with the literature [23]. Although the concentration of dopant is small, this characterization gives additional evidence for the successful doping of $Ag^+$ into the HAp lattices.

Figs. 4 and 5 show the SEM, TEM, elemental mapping, EDX, and SAED pattern of the pure HAp powder and Ag-HAp

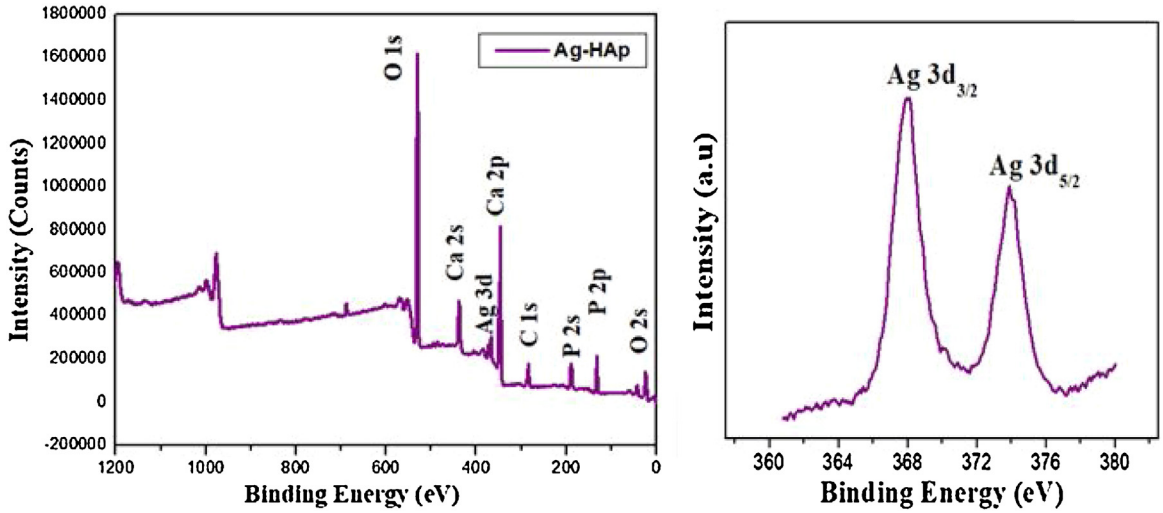


**Fig. 3 – XPS spectrum of Ag-HAp composite and Ag's elemental spectrum.**

composite respectively. The SEM image provides information about the particle size and typical shape for the as-prepared samples (Fig.4). It can be observed from the figures of both the samples, doped as well as pure HAp exhibits agglomeration, and can be seen that the doping of $Ag^{+}$ metal has considerable influence on the morphology of HAp powder. We noted from the morphology that the HAp samples prepared from the Ag-doping have much smaller particle size as against the pure HAp ones. Further, the EDX spectra and the elemental mapping confirms for the uniform distribution of Ag in the Ag-HAp sample along with elements of Ca, P, and O, and thereby confirming for the successful formation of Ag-HAp composite.

The TEM micrograph of pure HAp (Fig.4) shows the particles of non-uniform size distribution with elongated rod-like morphology with a spherical lump of around 50 nm size, while the Ag-HAp particles (Fig.5) exhibit simple small rod-shaped morphology. The length of the nanorods varied from 20–30 nm and the diameter was between 5–10 nm and the doped Ag-HAp sample is amorphous as seen in the SAED pattern and the bright spots diffuse to form rings. In one of the similar

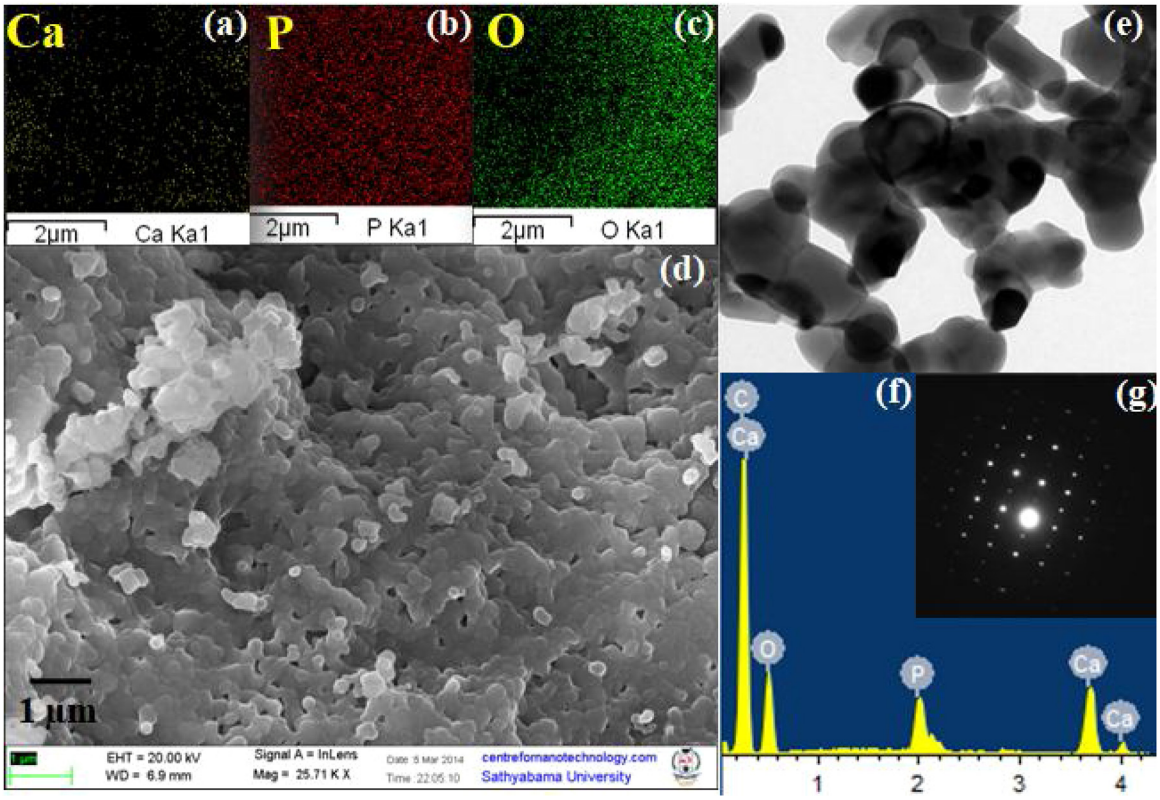


**Fig. 4 – SEM, elemental mapping, EDX, TEM, and SAED pattern of synthesized HAp nanopowder.**

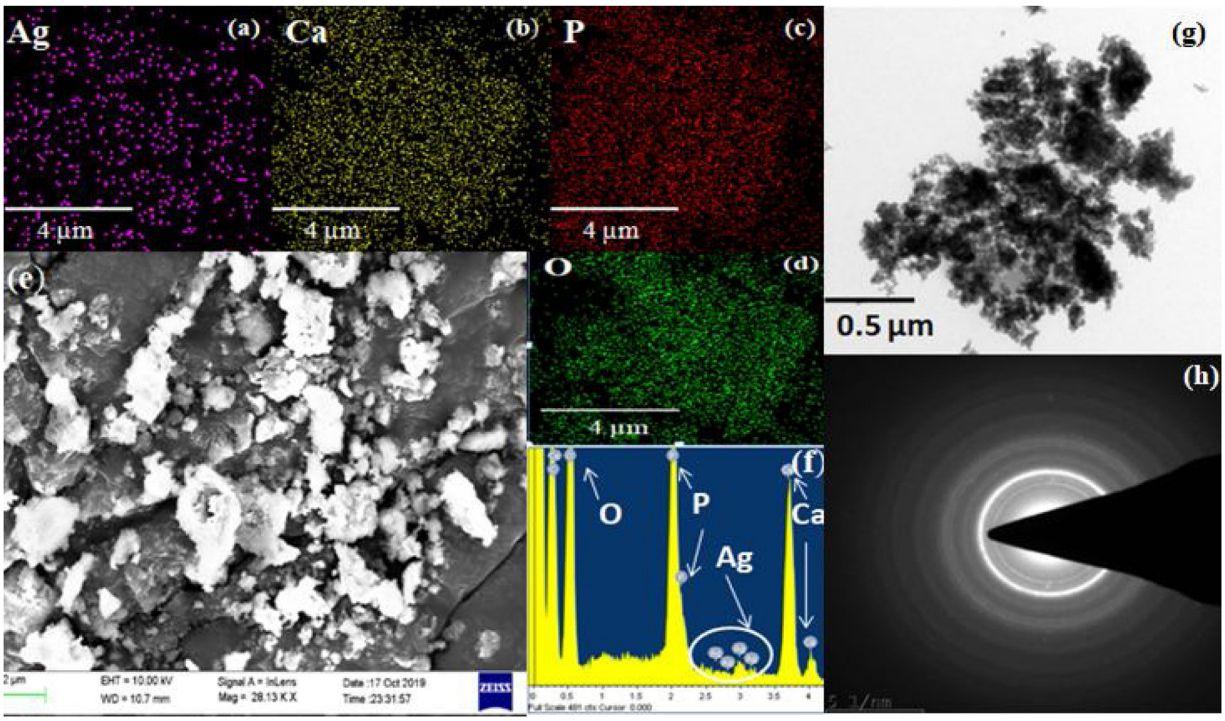


**Fig. 5 – SEM, elemental mapping, EDX, TEM, and SAED pattern of synthesized Ag-HAp nanopowder.**

study, Chung et al. (2006) reported for the presence of crystalline phase of $Ag_2O$ along with the HAp and nitrate phases and is strongly influenced by Ag's degree of substitution and in this, the formation of $Ag_2O$ nuclei did not seem to be detected [26].

Fig. 6 displays the stereo zoom optical images of pure HAp and Ag-HAp/PLA scaffold along with its EDX and SEM at different magnifications. From the figure (Fig. 6e), the scaffold-coated HAp sample seems to be exhibiting the highly open-porous structure, where the large pores are interconnected with each other. The size of macropores depends on the PLA framework, and it is easy to customize the scaffolds of desired shape and size as it is particularly required for some needs. Besides, the EDX provided elemental analysis (Fig. 6b,f) indicates the presence of all elements like Ca, P, C, O, and an additional element Ag for the doped HAp and thereby confirming for the successful formation of Ag-HAp/PLA scaffold. Also, the SEM provided morphologies (Fig. 6g–h) showed that all the coatings are compact, even, and contain aggregated granules at the surface, as compared against the pure HAp (Fig. 6c–d). The formation of such porous scaffolds by the HAp composite is the most promising material in particular for bone defects, repair, and tissue regeneration. Some of the earlier researches on scaffold materials have confirmed the same that the porous structures are essential criteria for the conduction of essential nutrients to help with the tissue growth [27].

It is well recognized that upon implantation, the adsorption of essential nutrients and proteins takes place on the biomaterial's exterior surface and this occurs by the regulation of diverse biological proceedings like biocompatibility, cell adhesion, immune responses, and associated blood coagulation [28]. Since the protein adsorption is a vibrant process and is also strongly influenced by the nature of the protein layers available at the surface of biomaterial, in addition to the topographical/textural/pore-size characteristics of the biomaterial. The mentioned biomaterial characteristics, in general, decides which proteins are capable to bind over the material [29]. It also assists the restriction/adsorption of certain proteins within the deformities of material's surface and observed that the type of adsorbed protein at the surface is simply affected by the characteristics of the underlying material, for example, the porous scaffold's physical and chemical properties restrict its adsorption capacity [30]. Taking into consideration these facts, the α-MEM with 10% FBS was used to assess the adsorption capacity of protein onto the pure HAp and Ag-HAp/PLA composites. As shown in Fig.7, the total amount of protein that got adsorbed onto the surfaces of the two materials are different and is attributed to the changes in the morphologies and constituents. The Ag-HAp/PLA sample supported the significantly high protein adsorption than that of corresponding pure HAp due to the availability of additional Ag constituent and PLA scaffolds that influences the crystallinity and porosity. Also, the surface of the Ag-HAp/PLA sample is uneven and impregnated with the active element that supports more protein adsorption. However, we see that the pure HAp material has protein adsorption capacity to some extent, but this can be dragged to a significant level by means of incorporating the Ag metal and with scaffolds, and thereby shifting to the promising levels. Further studies have to be performed to enlighten its biocompatibility as a promising scaffolding biomaterial.

Hemolysis is a vital aspect to evaluate the biocompatibility of material and the hemolytic assays are carried out to investigate the interaction of nanoparticles with the outer

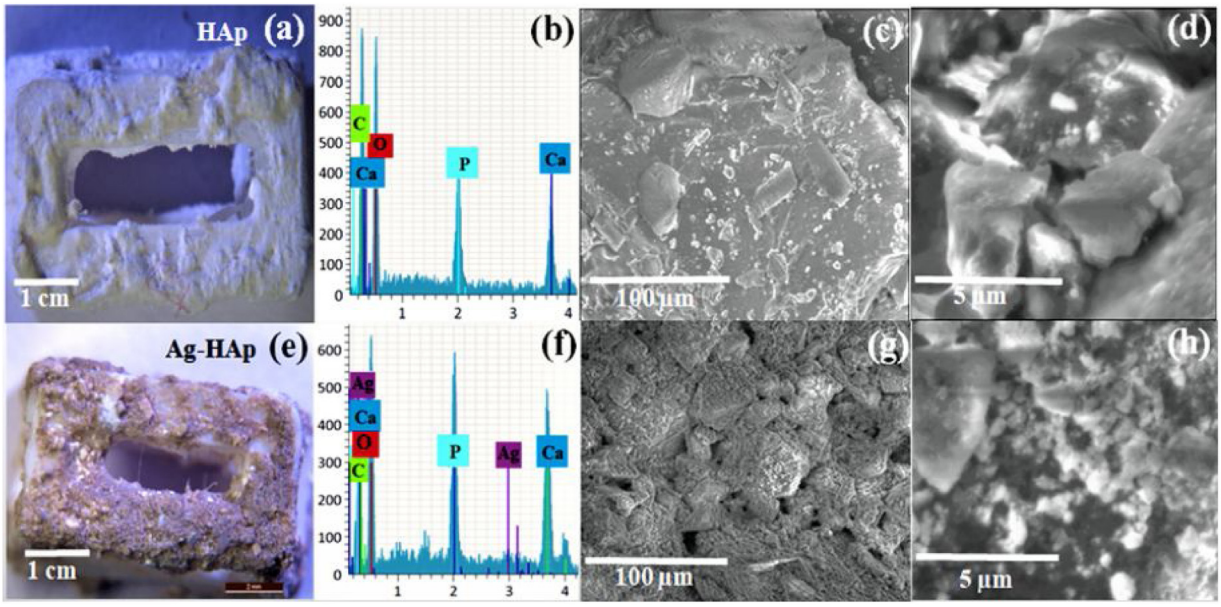


**Fig. 6 – (a,e) Optical images, (b,f) EDX spectrums, SEM images at 100 μm (c,g), and 5 μm (d,h) of pure HAp and Ag-HAp/PLA scaffold respectively.**

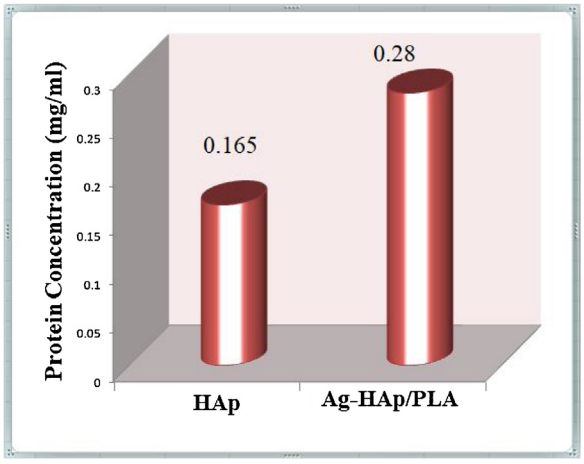


**Fig. 7 – FBS adsorption onto the surfaces of pure HAp and Ag-HAp/ PLA composite.**

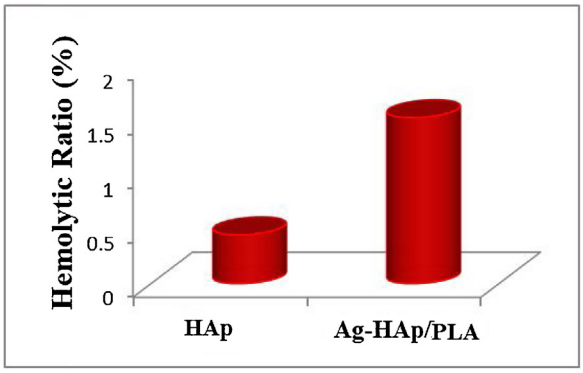


**Fig. 8 – Hemolytic assay comparison of pure HAp and Ag-HAp/PLA composite.**

membranes of the red blood cell by accessing the discharged hemoglobin [31]. Since the HAp particles interrelate with many copious cellular systems in our body, whilst a few of these interactions can perhaps lead to defective cells and kindle platelet activation, coagulation, and thrombus development [32,33]. Fig. 8 shows the hemolytic assay comparison of HAp and Ag-HAp/PLA composite. As per the ASTM F 756-00 guidelines, any sample with hemolysis rate less than 2% is considered to be non-hemolytic, and based on this, both of our HAp containing samples are considered to be the suitable materials for biomedical applications. From the testing, we found that the hemolysis rate of Ag-HAp/PLA composite found to be 0.8% greater than pure HAp, and still be considered as non-hemolytic as both of the sample's values are less than 2%. It can also be seen that the hemolysis ratio is strongly affected by the concentration of dopant and its degree of crystallinity, with the latter having a more dominating role towards the hemolysis [34].

The antimicrobial activity tests were conducted for the pure HAp and Ag-HAp/PLA composite against the bacteria *E. coli* (gram-negative) and *S. aureus* (gram-positive), where the analysis of results indicated the Ag-doped composite has higher inhibition of bacterial growth as against the un-doped ones. Also, within the Ag-doped composite, *E. coli* displayed more zone of inhibition (3 mm) in comparison with gram-positive bacteria (2 mm) and thereby signifying the stronger ability of *S. aureus* bacteria to fight against the toxic responses of the composite (Fig. 9). Also, the observation of no antibacterial activity for the pure HAp sample and is due to the absence of stronger antibacterial agent Ag in the sample. However, the observed difference of activity for the Ag-HAp/PLA composite among *E. coli* and *S. aureus* may be due to the differences in the cell wall responses against the Ag metal. Since *E. coli* has a

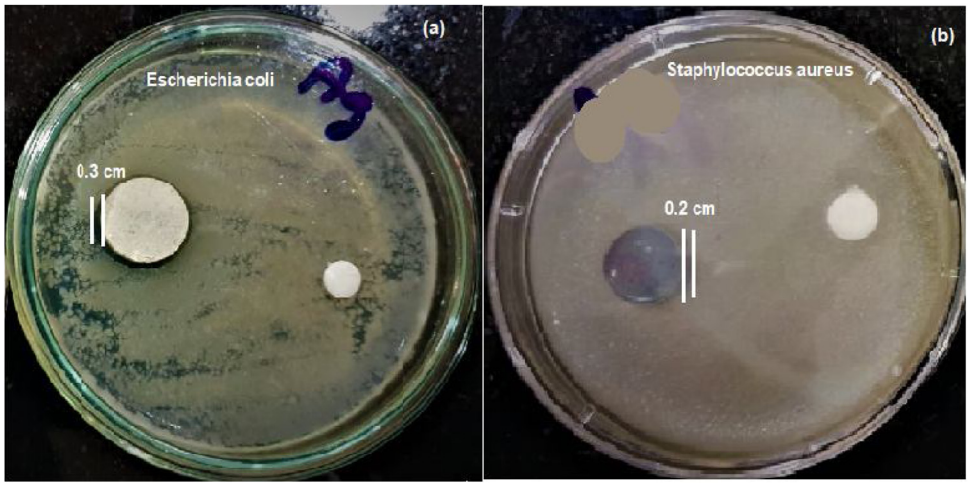


**Fig. 9 – Antibacterial assay of pure HAp and Ag-HAp/PLA composite against Gram-positive bacteria (*S. aureus*) and Gram-negative (*E. coli*).**

comparatively thinner cell wall (its associated characteristics) and the antioxidant enzymes (catalase) of *S. aureus* provided the sensitivity and stronger oxidant resistance (respectively) against the tested Ag-HAp/PLA composite [19].

Bone forms the skeleton system of the body and so any basic biomechanical requirements of the implanted scaffolding biomaterial include adequate bending, compression strength, appropriate to equalize the strength of a particular implant site. The mechanical characteristics of natural bone to a larger degree of extent fluctuate concerning age. Numerous researchers have reported that the reaction of the host to the implanted material is mainly driven by the mechanical as well as biological characteristics [35]. Researchers have conducted studies by combining polymers with ceramics to overcome the restrictions of polymers to improve its hydrophobic behavior as well as cell adhesion properties. In that view, the incorporation of PLA polymer for the implant applications has the additional advantage of decomposing the polymer itself into carbon dioxide, water, etc and in that way, there is no need to remove from the body [36]. The stress-strain analysis of the fabricated PLA scaffold (Fig. 10) by FDM proved

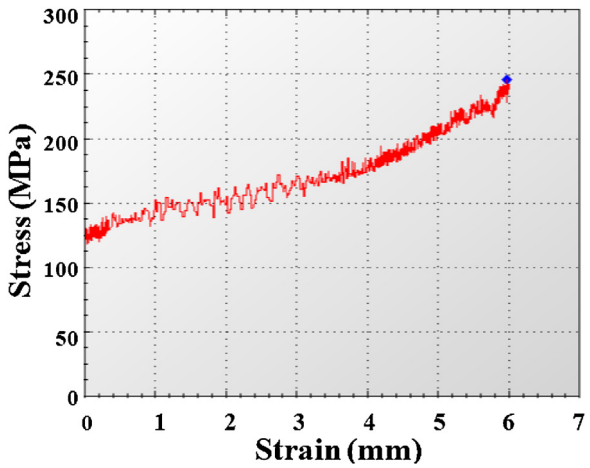


**Fig. 10 – The stress-strain analysis of Ag-HAp/PLA scaffold.**

to have a bending strength of approximately 125 MPa, comparable to the strength of cortical bone and so, it can be used for the load-bearing applications. The coating of the scaffold with biocompatible material improves its biocompatibility as demonstrated by hemolytic assay and protein adsorption studies. Therefore, the custom-made scaffolds to meet the requirements of individuals with desired shapes can be prepared by the FDM technique with ceramic polymer composite coating to meet the strength compatible with that of cortical bone.

## 5. Conclusion

This manuscript emphasizes a simple and effective way to amend the synthetic bio-inert PLA polymer scaffold (prepared by FDM technique) to a biocompatible scaffold by successfully coating the surface by Ag-HAp/PLA scaffold by simple dip coating. The XRD diffractogram reveals that there is an increase in crystallinity with a reduction in crystallite size as HAp is doped with silver. The XPS studies on Ag-HAp confirmed the incorporation of Ag on the crystal structure HAp, even though the concentration of Ag did not produce visible diffract gram produced by XRD. The successful formation of the composite was confirmed by the EDX analysis, while the morphology studies provided the shapes and sizes of the particles. The antibacterial activity of the composite powder showed greater inhibition efficiency towards *E. coli* better than *S. aureus* organisms. The *in vitro* hemocompatibility test of the Ag-HAp/PLA composite showed less than 2% of hemolytic activity and considered to be good compatibility with human blood. The *in vitro* protein adsorption test of the Ag-HAp/PLA composite showed moderate adsorption of FBS on the surface necessary for various nutrients transport. Finally, the hardness test confirms the scaffold bending strength is compatible with the cortical bone. Overall, based on the cumulative analysis of *in vitro* biological and hardness tests, it can be suggested that the fabricated nanocomposite coated Ag-HAp/PLA scaffold may serve as a potential polymeric biomaterial for bone tissue regeneration applications.

## Conflict of interest

The authors declare no conflicts of interest.

## Acknowledgments

This work was financially supported by the University of Malaya Research Grant (RU001-2019, RU001-2020). The King Saud University author is grateful to the Deanship of Scientific Research, King Saud University for funding through the Vice Deanship of Scientific Research Chairs..

## REFERENCES

[1] Lee M, Dunn JCY, Wu BM. Scaffold fabrication by indirect three-dimensional printing. Biomaterials 2005;26:4281–9.
[2] Shen H, Niu Y, Hu X, Yang F, Wang S, Wu D. A biomimetic 3D microtubule-orientated poly(lactide-co-glycolide) scaffold with interconnected pores for tissue engineering. J Mater Chem B 2015;3:4417–25.
[3] Frølich S, Weaver JC, Dean MN, Birkedal H. Uncovering nature's design strategies through parametric modelling, multi-material 3D printing, and mechanical testing. Adv Eng Mater 2017;19:1600848, 8 pp.
[4] Predoi D, Iconaru SL, Predoi MV, Motelica-Heino M, Guegan R, Buton N. Evaluation of antibacterial activity of zinc-doped hydroxyapatite colloids and dispersion stability using ultrasounds. Nanomaterials 2019;9:515, 22 pp.
[5] Zhu W, Li J, Leong YJ, Rozen I, Qu X, Dong R, et al. 3D-printed artificial micro fish. Adv Mater 2015;27:4411–7.
[6] Mironov V, Prestwich G, Forgacs G, et al. Tissue engineering by self-assembly and bioprinting of living cells. Biofabrication 2010;2:022001.
[7] Brydone AS, Meek D, Maclaine S. Bone grafting, orthopaedic biomaterials, and the clinical need for bone engineering. Proc Inst Mech Eng H 2010;224:1329–43.
[8] Iconaru SL, Prodan AM, Buton N, Predoi D. Structural characterization and antifungal studies of zinc-doped hydroxyapatite coatings. Molecules 2017;22:604, 13 pp.
[9] Ciobanu CS, Iconaru SL, Coustumer PL, Predoi D. Vibrational investigations of silver-doped hydroxyapatite with antibacterial properties. J Spectrosc 2013:471061, 5 pp.
[10] Tofail SAM, Koumoulos EP, Bandyopadhyay A, Bose S, O'Donoghue L, Charitidis C. Additive manufacturing: scientific and technological challenges, market uptake and opportunities. Mater Today 2018;21:22–3.
[11] Bose S, Ke D, Sahasrabudhe H, Bandyopadhyay A. Additive manufacturing of biomaterials. Prog Mater Sci 2018;93:45–111.
[12] Kalita SJ, Bose S, Hosick HL, Bandyopadhyay A. Development of controlled porosity polymer-ceramic scaffolds via FDM. Mater Sci Eng C 2003;23:611–20.
[13] Lett JA, Sundareswari M, Ravichandran K. Porous hydroxyapatite scaffolds for orthopedic and dental applications — the role of binders. Mater Today Proc 2016;3(6):1672–7.
[14] Alvarez-Barreto JF, Landy B, VanGordon S, Place L, DeAngelis PL, Sikavitsas VI. Enhanced osteoblastic differentiation of mesenchymal stem cells seeded in RGD-functionalized PLLA scaffolds and cultured in a flow perfusion bioreactor. J Tissue Eng Regen Med 2011;5(6):464–75.
[15] He C, Xiao G, Jin X, Sun C, Ma PX. Electrodeposition on nanofibrous polymer scaffolds: rapid mineralization, tunable calcium phosphate composition and topography. Adv Funct Mater 2010;20(20):3568–76.
[16] Predoi D, Iconaru SL, Predoi MV. Dextran-coated zinc-doped hydroxyapatite for biomedical applications. Polymers 2019;11:886, 16 pp.
[17] Yuan Q, Wu J, Qin C, Xu A, Zhang Z, Lin Y, et al. One-pot synthesis and characterization of Zn-doped hydroxyapatite nanocomposites. Mater Chem Phys 2017;199:122–30.
[18] Jadalannagari S, Deshmukh K, Ramanan SR, Kowshik M. Antimicrobial activity of hemocompatible silver doped hydroxyapatite nanoparticles synthesized by modified sol-gel technique. Appl Nanosci 2014;4:133–41.
[19] Fielding GA, Roy M, Bandyopadhyay A, Bose S. Antibacterial and biological characteristics of silver containing and strontium doped plasma sprayed hydroxyapatite coatings. Acta Biomater 2012;8:3144–52.
[20] Roy M, Fielding GA, Beyenal H, Bandyopadhyay A, Bose S. Mechanical, *in vitro* antimicrobial, and biological properties of plasma-sprayed silver-doped hydroxyapatite coating. ACS Appl Mater Interf 2012;4:1341–9.
[21] Gibson I, Rosen DW, Stucker B. Additive manufacturing technologies: rapid prototyping to direct digital manufacturing. 2nd ed. New York: Springer; 2010.
[22] Lv Y, Chen X, Wang Q, et al. Synthesis and characterization of chitosan-based biomaterials modified with different active groups and their relationship with cytotoxicity. J Wuhan Univ Technol Mater Sci Edit 2007;22: 695–700.
[23] Williamson GK, Hall WH. X-ray line broadening from filed aluminium and wolfram. Acta Metall 1953;1:22–31.
[24] Ciobanu CS, Iconaru SL, Chisriuc SC, Costescu A, Coustumer PL, Predoi D. Synthesis and antimicrobial activity of silver-doped hydroxyapatite nanoparticles. Biomed Res Int 2013;2013:916218, 10 pp.
[25] Ge M, Ge K, Gao F, et al. Biomimetic mineralized strontium-doped hydroxyapatite on porous poly(L-lactic acid) scaffolds for bone defect repair. Int J Nanomed Nanosurg 2018;13:1707–21.
[26] Chung RJ, Ming FH, Huang CW, Perng LH, Wen HW, Chin TS. Antimicrobial effects and human gingival biocompatibility of hydroxyapatite sol-gel coatings. J Biomed Mater Res B Appl Biomater 2006;76:169–78.
[27] Stanic V, Janackovic D, Dimitrijevic S, et al. Synthesis of antimicrobial monophase silver-doped hydroxyapatite nanopowders for bone tissue engineering. Appl Surf Sci 2011;257:4510–8.
[28] Tan J, Saltzman WM. Biomaterials with hierarchically defined micro- and nanoscale structure. Biomaterials 2004;25(17):3593–601.
[29] Horbett TA. Biomaterials: interfacial phenomena and applications. In: Cooper SL, Peppas NA, Hoffman AS, Ratner BD, editors. Advances in chemistry series. Washington DC: American Chemical Society; 1982.
[30] Vroman L, Adams AL, Fischer GC, Munoz PC, Standford M. In: Cooper SL, Peppas NA, Hoffman AS, Ratner BD, editors. Biomaterials: interfacial phenomena and applications. Washington DC: American Chemical Society; 1982.
[31] Lord MS, Foss M, Besenbacher F. Influence of nanoscale surface topography on protein adsorption and cellular response. Nano Today 2010;5:66–78.
[32] Xia W, Li J, Wang L, Huang D, Zuo Y, Yubao L. The release properties of silver ions from Ag-nHA/$TiO_2$/PA66 antimicrobial composite scaffolds. Biomed Mater 2010;5:044105.
[33] Quan R, Yang D, Wu X, Wang H, Miao X, Li W. *In vitro* biocompatibility of graded hydroxyapatite-zirconia composite bioceramic. J Mater Sci Mater Med 2008;19: 183–7.

[34] Wiessner J, Mandel G, Halverson P, Mandel N. The effect of hydroxyapatite crystallinity on hemolysis. Calcif Tissue Int 1988;42:210–9.
[35] Zhang T, Zhou S, Gao X, Yang Z, Sun L, Zhang D. A multi-scale method for modelling degradation of bioresorbable polyesters. Acta Biomater 2017;50: 462–75.
[36] Gibson LJ, Ashby MF, Harley BA. Cellular materials in nature and medicine. Cambridge, UK: Cambridge University Press; 2010.